

## EFFECTS OF VANE NUMBERS/TYPES ON THE SWIRLING FLOW FIELD CHARACTERISTICS OF A COUNTER-ROTATING RADIAL-RADIAL SWIRLER

Battal Gencer<sup>1</sup>  
Middle East Technical  
University  
Ankara, Turkey

Firat Kiyici<sup>2,3</sup>  
Tusas Engine Industries  
Inc.  
Eskisehir, Turkey

Mustafa Percin<sup>4,5</sup>  
Middle East Technical  
University  
Ankara, Turkey

### ABSTRACT

*This study explores the effect of number of vanes and vane type on the time-averaged and temporal flow fields of a confined counter-rotating radial-radial swirler experimentally in isothermal conditions. Five swirlers with different secondary swirler vane numbers and vane shapes which operate at a swirl number of 1.2 are tested at a Reynolds number of 35000. Velocity field measurements are conducted at the mid-plane of the swirlers via two-dimensional two-component (2D2C) particle image velocimetry (PIV) technique. Preliminary results for the baseline configuration reveal presence of a central toroidal recirculation zone (CTRZ) extending interior of the jet. Due to the presence of the CTRZ, the effective flow passage area is decreased and as a result, high axial jet velocities are observed at the exit of the jet. The results reveal that the presence of the square vanes instead of circular vanes causes the expansion angle to decrease slightly so the width of the recirculating flow decrease about 10% at 1.0Dh downstream distance from the swirler exit. Comparative analysis between the swirlers that have the same vane type but different vane numbers show that increasing the vane numbers (keeping the total flow passage area constant) does not have a significant effect on the size of the CTRZ as well as on the velocity magnitudes.*

### INTRODUCTION

Swirling flows are used in a range of applications such as internal combustion engines, industrial heaters, gas turbine combustors, and a variety of other devices [Gupta, 1984]. Main objectives of using three-dimensional highly-turbulent swirling flows in gas turbine combustors are to stabilize the flame, enhance clean combustion performance, and ensure quick mixing [Syred, 1972; Gupta, 1984]. The intensity of the swirl in swirling jet flows is characterized by the swirl number (SN), which is defined as the ratio of the axial flux of tangential momentum to axial flux of axial momentum [Beér, 1972]. Above some critical swirl number, an adverse axial pressure gradient and associated central toroidal recirculation zone (CTRZ) form, which is beneficial in terms of enhancing the mixing and flame stabilization. On the other hand, flows with high swirl numbers are prone to develop instabilities that may adversely influence the

---

<sup>1</sup> GRA in Aerospace Engineering Department at METU, Email: [bgencer@metu.edu.tr](mailto:bgencer@metu.edu.tr)

<sup>2</sup> Graduate Student in Aerospace Engineering Department at METU, Email: [e239229@metu.edu.tr](mailto:e239229@metu.edu.tr)

<sup>3</sup> Lead Combustion Aerodynamics Engineer in Tusas Engine Industries Inc., Email: [firat.kiyici@tei.com.tr](mailto:firat.kiyici@tei.com.tr)

<sup>4</sup> Asst. Prof. in Aerospace Engineering Department at METU, Email: [mpercin@metu.edu.tr](mailto:mpercin@metu.edu.tr)

<sup>5</sup> Exp. Aero. Lab. Coordinator in Center for Wind Energy Research (RÜZGEM), METU

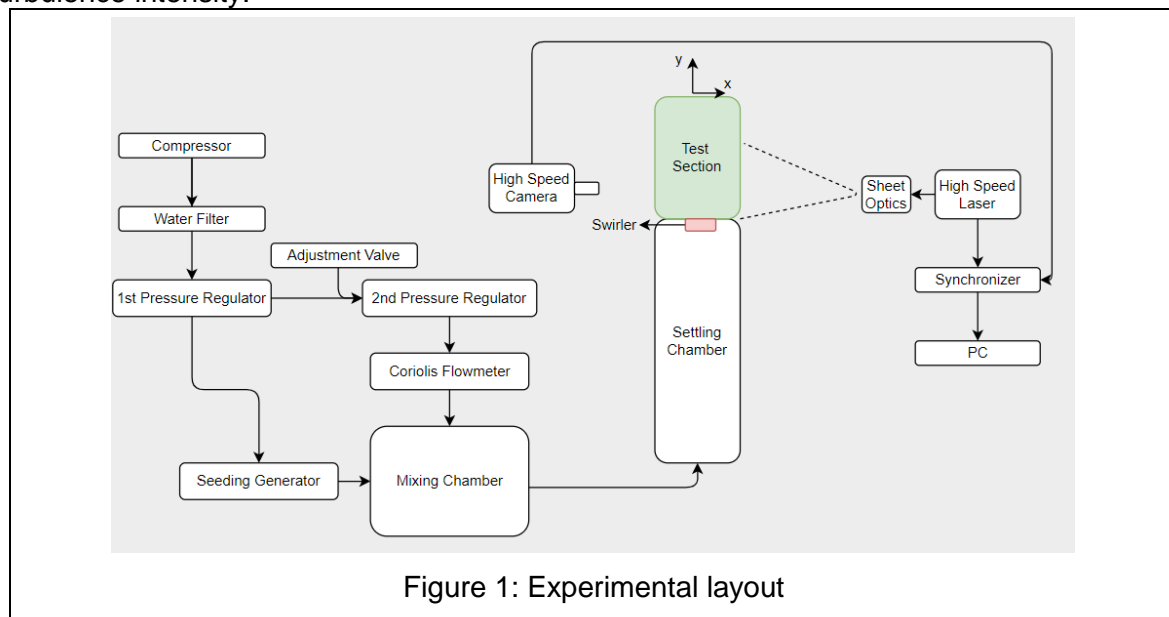
combustion efficiency [Syred, 1972; Syred, 2006]. Therefore, swirlers should be designed in such a way that they can create central recirculation zone of the desired size and shape while not causing combustion instabilities.

In this context, many experimental studies have been carried out in order to examine the effect of the boundary conditions on the mean and dynamic behavior of swirling flow. Fu et al. [2007] employed two-component Laser Doppler Anemometry (LDA) technique to investigate the mean velocity components and Reynolds stresses at downstream of a counter-rotating radial-radial swirler for confined and unconfined conditions. The size of the CTRZ was observed to be almost two times larger in the confined case compared to the unconfined case. It is also reported that turbulence activity is stronger for the unconfined case in the regions close to the swirler exit and near the swirler centerline. On the other hand, high turbulence intensity values are present in the near-wall regions at relatively downstream locations in the confined case [Fu et al., 2007]. The effect of the dome geometry on the flow field characteristics of a counter-rotating radial swirler was studied by Kao et al. [2013] by using two-component LDA technique. Three different dome geometries with expansion angles (angle between the dome surface and axis of swirler) of  $45^\circ$ ,  $60^\circ$  and  $90^\circ$  were tested for the same inlet conditions. They concluded that for the sudden expansion ( $90^\circ$ ) case, the swirling jet flow detaches from the dome surface whereas it stays attached to dome surfaces for the  $45^\circ$  and  $60^\circ$  cases. The dome geometry mainly affects the mean velocity profile in the regions closer to swirler exit [Kao et al., 2013]. In another study by Kao et al. [2013], the effect of chamber length with converging exhaust is analyzed for the same type of swirler. Three different chambers (all including downstream exhaust nozzle) with the lengths of 1.5, 2 and 3 times of the chamber width were tested and it was found that the shorter chamber length causes a favorable pressure gradient along the swirler axis and as a result greater axial and tangential velocity profiles are detected near the swirler exit [Kao et al., 2013]. Kao et al. [2014] also compared axial-radial (AR) and radial-radial (RR) type swirlers under similar boundary conditions. It is stated that the CTRZ is open-shape and the jet expansion angle is much higher for the RR type swirler when compared to the AR type swirler [Kao et al., 2014]. Lin et al. [2016] studied the effects of chevrons on the dynamic response of the flow field using high speed two-dimensional two-component (2D2C) Particle Image Velocimetry (PIV) measurements. Three different swirler configurations (without chevrons, 8 chevrons on the primary swirler- no chevron on the secondary swirler, 8 chevrons on the primary swirler-12 chevrons on the secondary swirler) were used. Swirler configuration with no chevrons caused the expansion angle be much higher compared to configurations with chevrons. It is also stated that the axial momentum of swirling jet decays faster for the configuration that has 8 chevrons on the primary swirler and 12 chevrons on the secondary swirler as a result of additional mixing generated by these sets of chevrons [Lin et al., 2016]. Reddy et al. [2005] conducted PIV measurements to investigate the flow field characteristics of a gas turbine combustor and found that decreasing the pressure drop through swirler from 0.1 bar to 0.05 bar causes the CTRZ length to drop from 4D to 3D and CTRZ width to drop from 2.25D to 1.87D where D is the outer diameter of swirler. Estefanos et al. [2015] studied the effects of flare angles and they concluded that the position of the shear layers thus the position of high turbulence and unsteadiness associated with the precessing vortex core (PVC) can be changed by changing the flare angle. In another study in which the effect of venturi geometry on the combustion behavior using counter-rotating RR swirler was analyzed, it is found that the converging venturi appears to perform better when it comes to eliminate the combustion instabilities and it is more effective in reducing the frequency coupling between the acoustic oscillations and heat release rate [Lin et al., 2017].

It is clear from the literature review that although the effects of numerous geometrical parameters have been studied, the influence of number of vanes and vane type on the swirling jet flows remains mostly unresolved. In this context, it is aimed to investigate the effect of vane numbers and vane types on the flow field characteristics of counter-rotating radial-radial type swirlers in isothermal conditions experimentally. In addition to detailed investigation of the time-averaged flow fields of the swirling jet flow, this experimental data serves as a validation basis for numerical simulations.

## EXPERIMENTAL SETUP AND PROCEDURE

Experiments are performed in the Experimental Fluid Dynamics Laboratory of METU Center of Wind Energy Research (RÜZGEM). The experimental layout and experimental setup are shown in Figure 1 and Figure 2, respectively. Air is supplied from a pressurized air tank (nearly at 8 bars) and first passes through a dehumidification system. Subsequently, the air pressure is reduced to 6 bars in the first pressure regulator which directs the air to a Coriolis type flow meter (Micro Motion F050S) and a seeding generator (single-jet Laskin nozzle). The second pressure regulator that is placed upstream of the flow meter is used to adjust the mass flow rate to 12.9 g/s. This main airstream is mixed with seeding particles (oil olive droplets with 1  $\mu\text{m}$  diameter) in a mixing chamber. The air-seeding particle mixture then flows through a settling chamber (with a cross-section dimensions of 12 cm x 12 cm and a length of 120 cm) that also includes a turbulence screen in order to generate a uniform velocity profile with a relatively low turbulence intensity.



The hydraulic diameter is defined as the outer diameter of the secondary swirler, which is  $D_h=2.8$  cm. Tests were performed at the air mass flow rate of 12.9 g/s corresponding to a Reynolds number of 35.000 based on the hydraulic diameter and the mean swirler exit velocity ( $V_{\text{exit}}=17.46$  m/s). The test section (viz. confinement) is produced from PlexiGlas material to allow for optical access. It has cross-section dimensions of 12 cm x 12 cm and a total length of 60 cm.

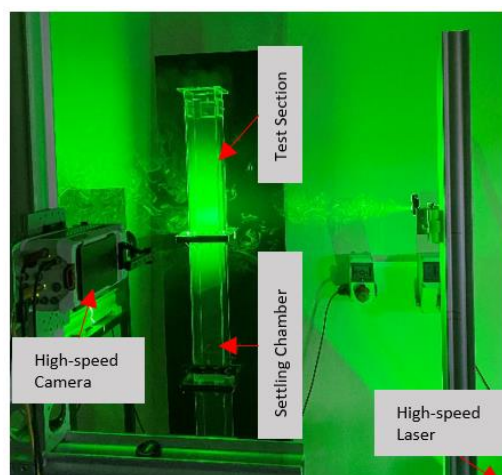


Figure 2: Experimental Setup

Properties of the five swirlers that are tested in this study and an additional swirler which was studied by Kiyici et al. [2021] are given in Table 1. All of the swirlers consist of two stages and they are designed to operate at same swirl number. The reader is referred to Kiyici et al. [2021] for further details regarding the swirler geometry. When viewed from the swirler exit, the primary swirler is designed to rotate the flow in the counterclockwise direction while the secondary swirler rotating the flow in the clockwise direction.

Table 1: Swirler configurations considered in this study

| Swirler Name              | Number of Vanes at Primary Swirler | Number of Vanes at Secondary Swirler | Vane Type |
|---------------------------|------------------------------------|--------------------------------------|-----------|
| 810C                      | 8                                  | 10                                   | Circular  |
| 810S                      | 8                                  | 10                                   | Square    |
| 812C (Baseline)           | 8                                  | 12                                   | Circular  |
| 812S Kiyici et al.[ 2021] | 8                                  | 12                                   | Square    |
| 816C                      | 8                                  | 16                                   | Circular  |
| 816S                      | 8                                  | 16                                   | Square    |

2D2C high speed PIV system is used to obtain velocity fields in the mid-plane of the swirler. Litron LDY300 high-speed laser (with a wavelength of 527 nm) is used for the illumination of the measurement plane. Images of tracer particles are recorded by a Phantom V640 high-speed camera, which has 2560x1600 pixels of maximum resolution. Camera is synchronized with the laser by the use of a synchronizer (TSI Model 610036). 2000 double-frame images are captured at recoding frequency of 200 Hz to allow for a converged statistical analysis by using statistically independent samples and capturing the flow for enough period of time. The time interval between frames is set to be 10  $\mu$ s. The field of view covers 13 cm in the radial direction (i.e., the x direction) and 20.8 cm in axial direction (i.e., the y direction) which allowed us to capture enough distance at downstream of the swirler. TSI software Insight 4G is used for the data acquisition and necessary processing steps including processing, vector calculation and post-processing steps. To improve the contrast of the particle images, background intensity subtraction and image filtering with a 5x5 Gaussian kernel are used. The double-frame images are interrogated using cross-correlation technique over an interrogation area size of 32 pixels  $\times$  32 pixels with 50% overlap. The resultant vector spacing is 1.3 mm.

## RESULTS

### General Flow Pattern

In this part, results for the baseline swirler (8 radial circular vanes in the primary swirler and 12 radial circular vanes in the secondary swirler) which is denoted as 812C are presented. Both y-component (velocity in the axial direction, V) and x-component (velocity in the radial direction, U) of velocity are normalized with the bulk velocity ( $V_0$ ) which is measured as 0.89 m/s at an upstream location of the swirler in the settling chamber.

Normalized y-velocity contours for 812C swirler are shown in Figure 3a. The expansion angle which is the angle between the swirler axis and the location where the flow interacts with the side walls is approximately 45°. The axial velocity values are maximum at the exit of the swirler and there exists a prominent recirculation zone (i.e., CTRZ) aligned with the central axis of the swirler. The length of the CTRZ exceeds the field of view of the camera. The flow attaches the side walls at around  $y/D_h > 1.1$  as evident from Figure 3a. Due to the presence of the CTRZ, the effective flow passage area is decreased and as a result, high axial jet velocities are observed at regions close exit of the jet.

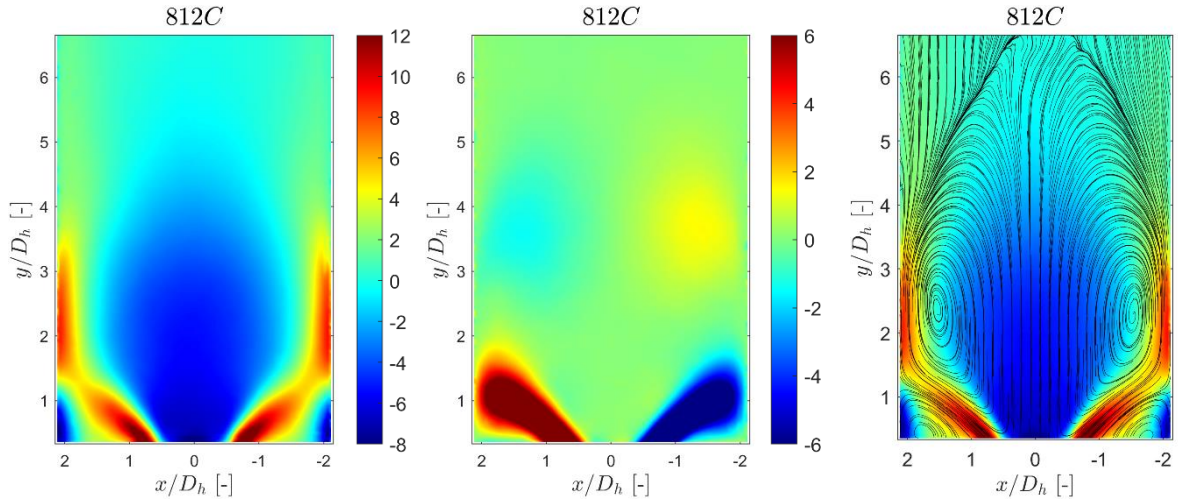


Figure 3: (a) Contours of normalized time-averaged y-velocity ( $\bar{V}/V_0$ ) (left); (b) contours of normalized time-averaged x-velocity ( $\bar{U}/V_0$ ) (middle); (c) contours of normalized time-averaged y-velocity ( $\bar{V}/V_0$ ) with streamlines (right)

Figure 3b presents the velocity field for the normalized mean radial velocity component of the flow. The expansion of the jet flow is axisymmetric. For  $y/D_h > 3$ , the near-wall flow is directed slightly towards the central axis of the jet, that is in agreement with the maximum width location of the CTRZ. This behavior is seen more clearly in Figure 3c that provides the axial velocity contours complemented with streamlines. It can be clearly seen that a massive CTRZ occurs suggesting presence of an adverse pressure gradient in the axial direction. Moreover, there are corner recirculation zones under the expanded jet region.

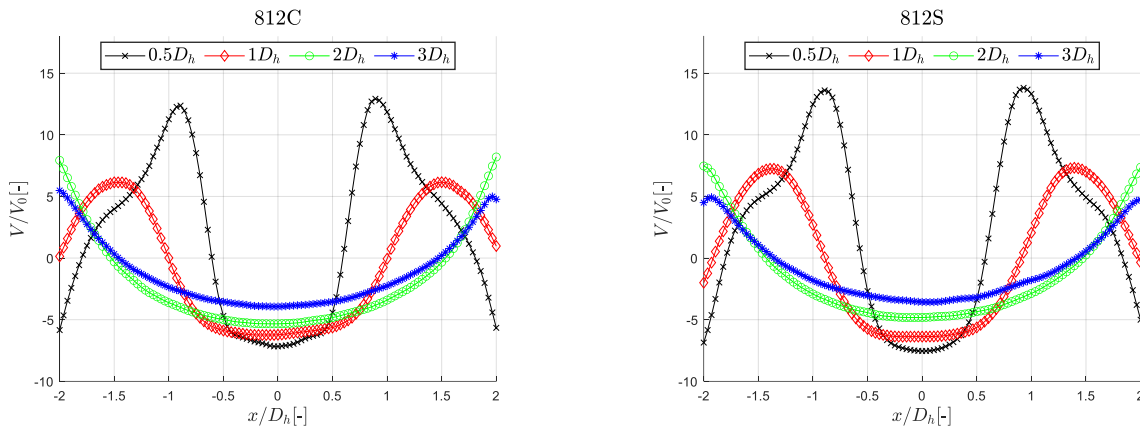


Figure 4: (a) Normalized mean axial velocity profiles at different streamwise locations for 812C swirler (left); (b) for 812S [Kiyici et al., 2021] swirler (right)

Axial velocity profiles at different streamwise positions are extracted and plotted in Figure 4a and Figure 4b for 812C and 812S (Kiyici et al. [2021]), respectively. The expansion of the swirling jet is evident from the velocity profiles for  $y/D_h = 0.5$  and  $y/D_h = 1.0$ . Moreover, the velocity magnitude decreases after  $y/D_h > 1$  and the swirling jet flow becomes a wall jet near the confinement walls. Here, it can be said that the streamwise velocity profile for the 812S (Kiyici et al., [2021]) swirler has the same trend compared to 812C swirler but the peak of the velocity values at  $y/D_h = 0.5$  and  $y/D_h = 1$  is relatively higher whereas it becomes almost the same at  $y/D_h = 2$  and  $y/D_h = 3$ . Moreover, the radial distance between the peak velocity values at  $y/D_h = 0.5$  and  $y/D_h = 1$  is greater for 812C swirler. For example, the peak values are obtained at  $x/D_h = \pm 1.45$  for the 812C swirler, whereas it is at  $x/D_h = \pm 1.35$  for 812S (Kiyici et al., [2021]) swirler at  $y/D_h = 1$ . These differences are discussed in more detail in the following section.

### Effect of Vane Types

In this part, the effect of vane types (circular or square) on flow field characteristics is investigated. In this context, swirlers with the same vane number were compared. Figure 5, shows the comparison of normalized time-averaged y-velocity ( $\bar{V}/V_0$ ) profiles at the streamwise downstream distance of  $1.0D_h$  of swirlers with the same number of vane but different vane types.

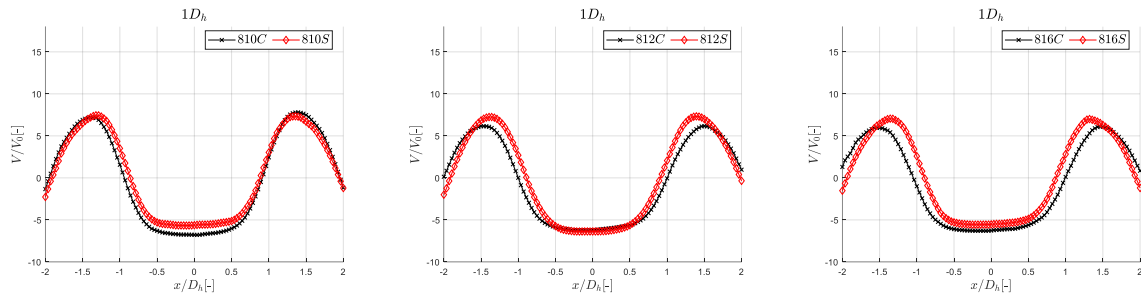


Figure 5: (a) Comparisons of the normalized axial velocity profiles at streamwise downstream distance of  $1D_h$  between 810C and 810S (left); (b) between 812C and 812S [Kiyici et al., 2021] (middle); (c) between 816C and 816S (right)

Figures 5a, 5b and 5c show the comparison between swirlers 810C-810S, 812C-812S (Kiyici et al. [2021]) and 816C-816S, respectively. As can be seen, at  $1.0D_h$  downstream distance from the swirler exit, the expansion angle in the circular-vane swirler is slightly higher than the square-vane swirler. However, the overall flow pattern becomes almost identical at further streamwise downstream locations. Figure 6a, 6b and 6c present the comparisons of the same velocity profiles at  $2.0D_h$  downstream location from the swirler exit. The velocity profiles at this downstream location are similar to each other, unlike those at  $1.0D_h$  distance, and this similarity continues at further downstream distances (i.e.  $3.0D_h$ ,  $4.0D_h$ ).

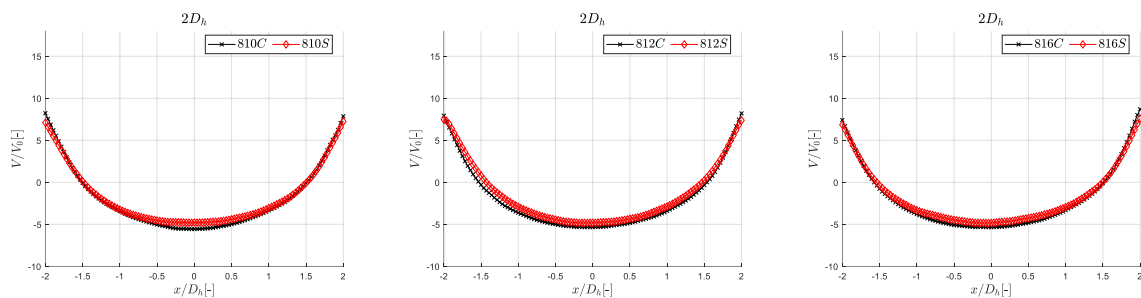


Figure 6: (a) Comparisons of the normalized axial velocity profiles at streamwise downstream distance of  $2.0D_h$  between 810C and 810S (left); (b) between 812C and 812S [Kiyici et al., 2021] (middle); (c) between 816C and 816S (right)

Normalized turbulent kinetic energy ( $TKE/V_0^2$ ) contours for 810C, 810S, 816C and 816S swirler are shown in Figure 7. These contours are related to the inner and outer shear layers where the inner shear layer is formed between two swirl flows, the outer shear layer is formed between the outer swirl and the environment. Contours of turbulent kinetic energy display similar patterns regardless of the vane shape yet the increased distance between inner shear layers close to the swirler exit for circular-vane swirler suggests slightly higher expansion angle.

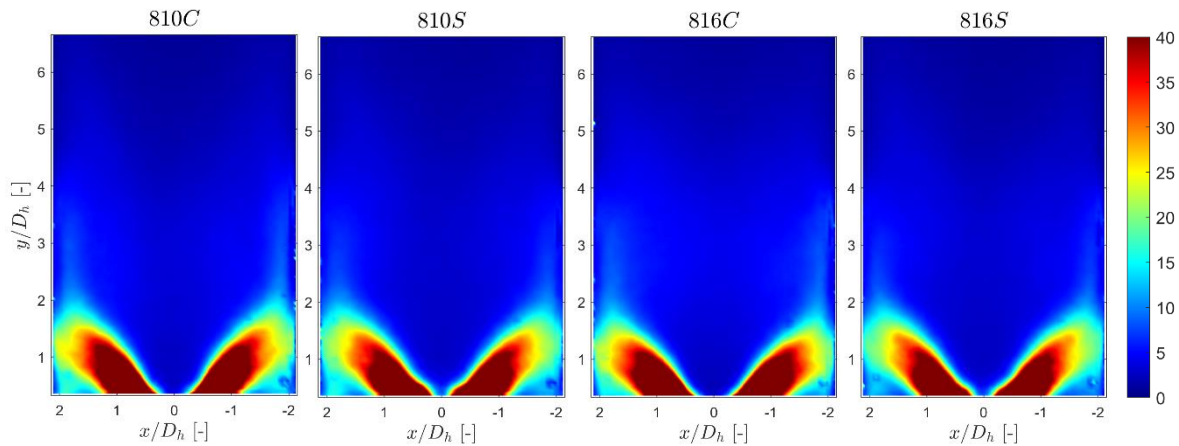


Figure 7: Contours of the normalized turbulent kinetic energy ( $TKE/V_0^2$ ) for different swirlers (from left to right; 810C, 810S, 816C, 816S, respectively)

Contours of normalized time-averaged y-velocity ( $\bar{V}/V_0$ ) with streamlines for all five swirlers are presented in Figure 8. Although the general flow fields seem to be similar, there are some differences while changing the vane type from square to circular. Firstly, it changes the expansion angle slightly as previously discussed. Secondly, it has an effect on the size of the CTRZ. As it is seen, the width of the CTRZ becomes smaller for  $y/D_h > 4$  for circular-vane swirlers compared to square-vane swirlers. At  $y/D_h = 6$  the width of the CTRZ is around  $1.95D_h$  for the 816C swirler whereas it is around  $2.1D_h$  816S swirler. This is an evident that the length of the CTRZ is also smaller for circular-vane swirlers.

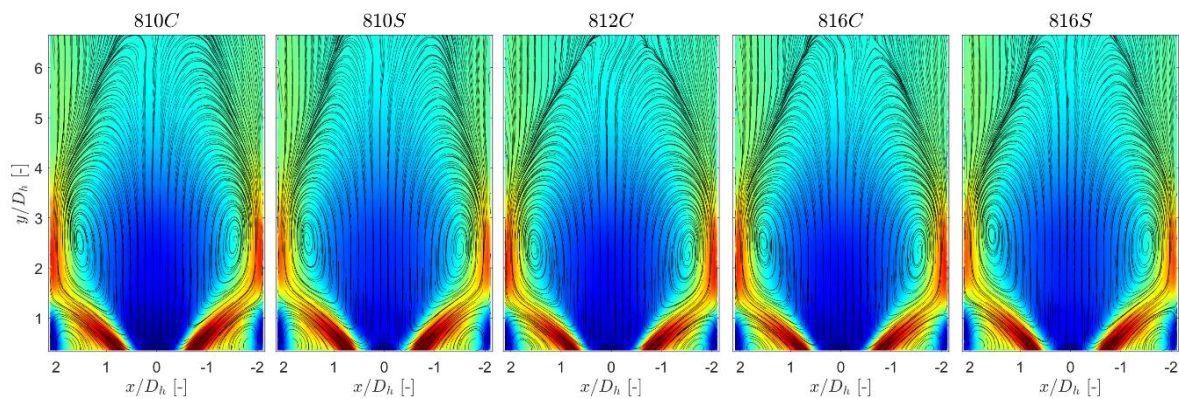


Figure 8: Contours of normalized time-averaged y-velocity ( $\bar{V}/V_0$ ) with streamlines for all five swirlers (from left to right; 810C, 810S, 812C, 816C, 816S, respectively)

### Effect of Vane Numbers

In this section, the effect of vane numbers on flow field characteristics is examined. For this purpose, in order to evaluate the effect of vane numbers, swirlers with the same vane types are divided into two parts, 810C-812C-816C and 810S-812S (Kiyici et al. [2021])-816S, and velocity profiles from  $1.0D_h$  and  $2.0D_h$  streamwise distances were extracted and shown in Figure 9 and Figure 10, respectively.

Figure 9a displays the comparisons between circular-vane swirlers where 9b represents the square-vane swirlers at  $y/D_h = 1.0$ . It is seen that increasing the vane number does not have much effect on the square-vane swirlers where it does have a very small effect on the

circular-vane swirlers. Figure 10 and Figure 11 shows that the velocity profiles become almost identical at further downstream locations.

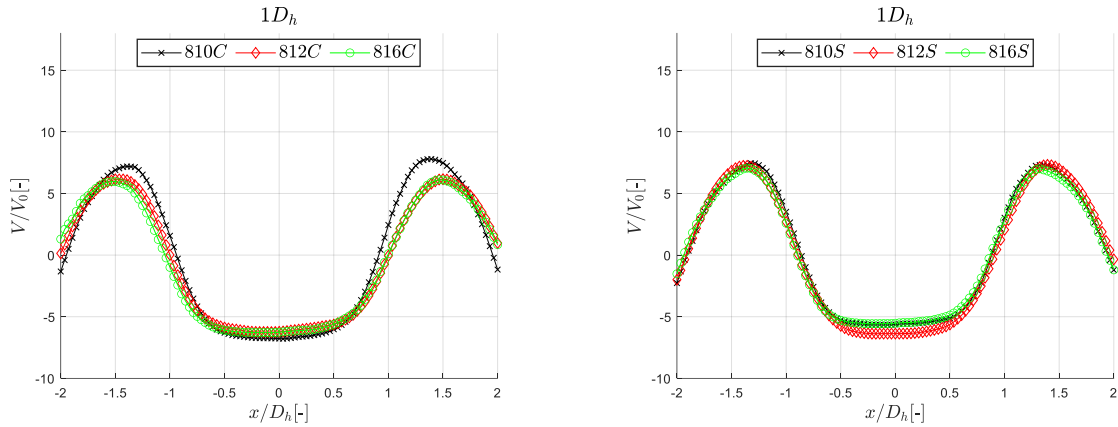


Figure 9: (a) Comparisons of the normalized axial velocity profiles at streamwise downstream distance of  $1D_h$  between 810C,812C and 816C(left); (b) between 810S, 812S [Kiyici et al., 2021] and 816S (right)

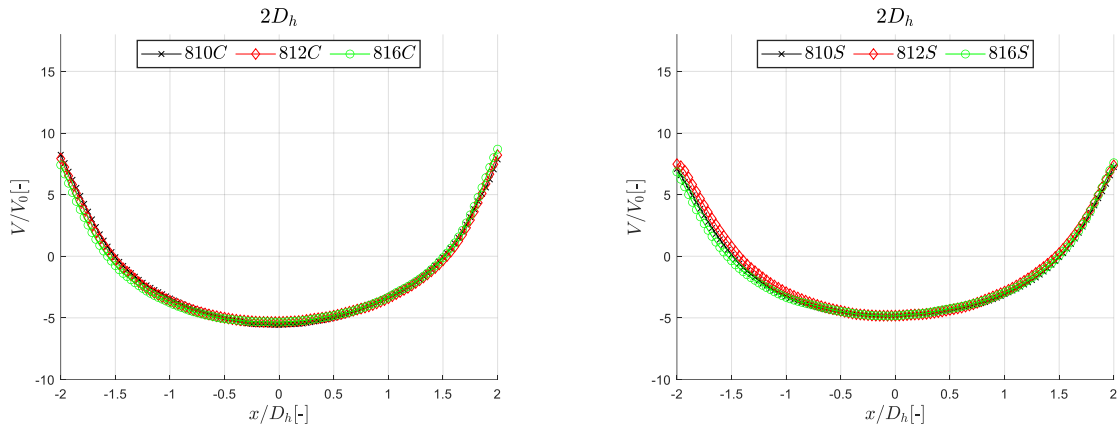


Figure 10: (a) Comparisons of the normalized axial velocity profiles at streamwise downstream distance of  $2.0D_h$  between 810C,812C and 816C(left); (b) between 810S, 812S [Kiyici et al., 2021] and 816S (right)

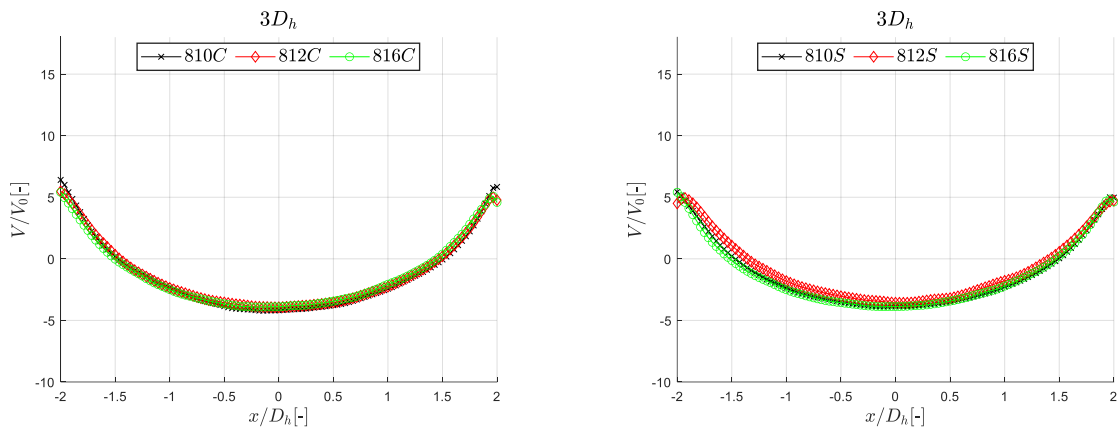


Figure 11: (a) Comparisons of the normalized axial velocity profiles at streamwise downstream distance of  $3.0D_h$  between 810C,812C and 816C(left); (b) between 810S, 812S [Kiyici et al., 2021] and 816S (right)

Normalized streamwise velocity contours, normalized radial velocity contours, normalized streamwise velocity contours with streamlines and normalized turbulent kinetic energy contours for all five swirlers that are tested in this study are presented in appendices part.

### CONCLUSIONS

In this study, the effects of number of vanes and vane type on the flow fields of a confined counter-rotating radial-radial swirler are experimentally investigated in isothermal conditions using 2D2C PIV measurements. Results for baseline swirler (812C) indicate the existence of CTRZ which is related to presence of an adverse pressure gradient in the axial direction. The efficient flow passage area is reduced due to the presence of the CTRZ, and as a result, high axial jet velocities are observed near the jet's exit.

The results reveal that the presence of the square vanes instead of circular vanes causes the expansion angle to decrease slightly so the width of the recirculating flow decrease about 10% at  $1.0D_h$  downstream distance from the swirler exit. This behaviour is also realized in the normalized TKE contours. Until the streamwise downstream distance of  $4.0D_h$  the velocity profiles and the width of the CTRZ remains almost identical. However, at further downstream distances the width of the CTRZ becomes smaller for the circular-vane swirlers compared to square-vane swirlers. This indicate that the presence of circular vanes reduces the length of the CTRZ slightly.

Comparative analysis between the swirlers that have the same vane type but different vane numbers show that increasing the vane numbers (keeping the total flow passage area constant) does not have a significant effect on the size of the CTRZ as well as on the velocity magnitudes.

### ACKNOWLEDGEMENTS

The authors are thankful to TUSAS Engine Industries Inc. for their monetary assistance (TEI) and also appreciate the technical assistance offered by the RÜZGEM staff during the tests.

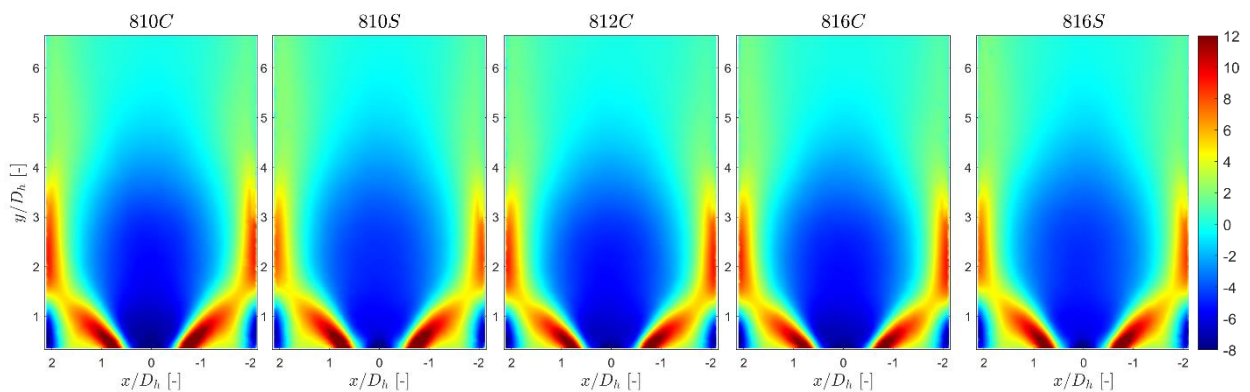
### References

- Beér, J. M., & Chigier, N. A. (1972). *Combustion Aerodynamics*. New York: Halsted Press Division, Wiley.
- Estefanos, W., Tambe, S., & Jeng, S. (2015). Effect of the Flare Expansion Angle on the Mean and Dynamic Behavior of Swirling Flow Generated by a Counter Rotating Radial-Radial Swirler Using a Water Test Rig. *Volume 4B: Combustion, Fuels and Emissions*. doi:10.1115/gt2015-43470
- Fu, Y., Cai, J., Jeng, S., & Mongia, H. (2007). Characteristics of the Swirling Flow Generated by a Counter-Rotating Swirler. *43rd AIAA/ASME/SAE/ASEE Joint Propulsion Conference & Exhibit*. doi:10.2514/6.2007-5690
- Gupta, A. K., Lilley, D. G., & Syred, N. (1984). *Swirl Flows*. Tunbridge Wells: Abacus.
- Kao, Y., Haseman, J. B., Tambe, S. B., & Jeng, S. (2014). Aerodynamics Comparisons Between Two Typical Gas Turbine Combustion Swirlers. *Volume 4B: Combustion, Fuels and Emissions*. doi:10.1115/gt2014-26137
- Kao, Y., Tambe, S. B., & Jeng, S. (2013). Effect of Chamber Length with Converging Exhaust On Swirling Flow Field Characteristics of a Counter-Rotating Radial-Radial Swirler. *Volume 1B: Combustion, Fuels and Emissions*. doi:10.1115/gt2013-95345
- Kao, Y., Tambe, S. B., & Jeng, S. (2013). Effect of Dome Geometry On Swirling Flow Field Characteristics of a Counter-Rotating Radial-Radial Swirler. *Volume 1B: Combustion, Fuels and Emissions*. doi:10.1115/gt2013-95344
- Kiyici, F., Percin, M. (2021). Experimental Investigation of the Confinement Effects in Radial-Radial Swirlers. ASME Turbo Expo 2021: *Turbomachinery Technical Conference and Exposition, Virtual, Online*.

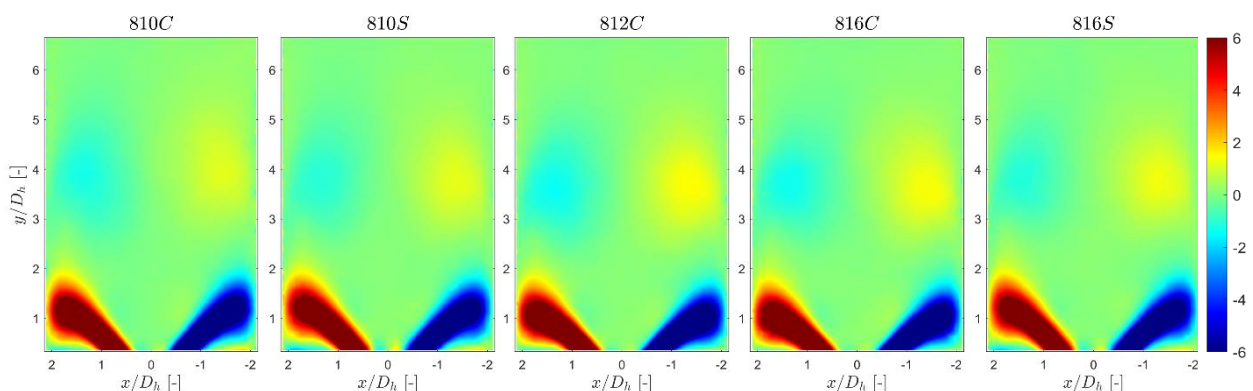
- Lefebvre, A. H., & Ballal, D. R. (2010). *Gas Turbine Combustion: Alternative Fuels and Emissions*. Boca Raton: CRC Press.
- Lin, S., Estefanos, W., Brennan, J., Tambe, S., & Jeng, S. (2016). The Effect of Chevrons on the Primary and Secondary Swirlers on the Dynamic Behavior of the Flow Generated by a Counter-Rotating Radial-Radial Swirler. *Volume 4A: Combustion, Fuels and Emissions*. doi:10.1115/gt2016-56622
- Lin, S., Wang, X., Estefanos, W., Tambe, S., & Jeng, S. (2017). The Effect of the Geometric Modifications of the Venturi on the Non-Reactive Flow and Combustion Behavior Using a Counter-Rotating Radial-Radial Swirler. *Volume 4B: Combustion, Fuels and Emissions*. doi:10.1115/gt2017-64876
- Reddy, P. R., Sujith, R., & Chakravarthy, S. (2005). Swirler Flow Field Characteristics in a Sudden Expansion Combustor Geometry Using PIV. *43rd AIAA Aerospace Sciences Meeting and Exhibit*. doi:10.2514/6.2005-217
- Syred, N. (2006). A Review of Oscillation Mechanisms and the Role of the Precessing Vortex Core (PVC) in Swirl Combustion Systems. *Progress in Energy and Combustion Science*, 32(2), 93-161. doi: 10.1016/j.pecs.2005.10.002
- Syred, N., & Beér, J. (1974). Combustion in Swirling Flows: A Review. *Combustion and Flame*, 23(2), 143-201. doi:10.1016/0010-2180(74)90057-1

## APPENDICES

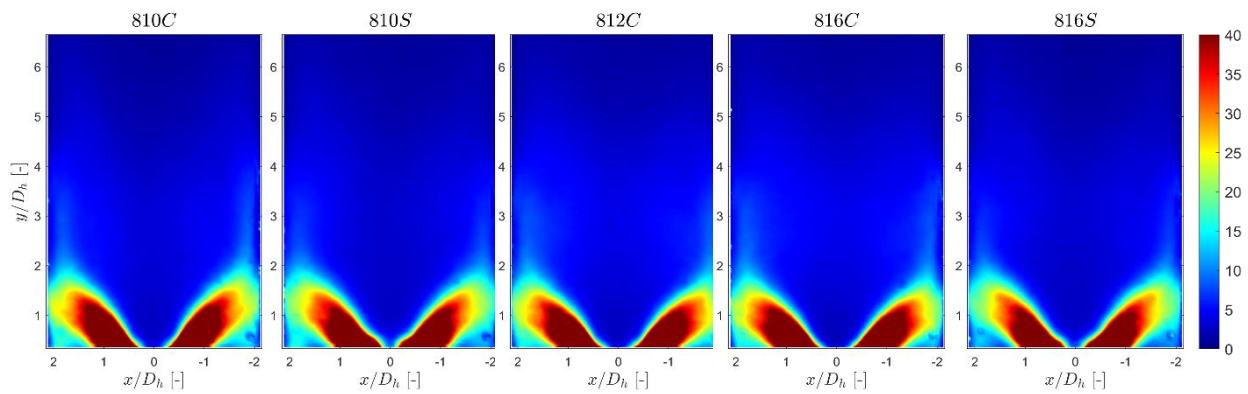
**Appendix 1:** Contours of normalized time-averaged y-velocity ( $\bar{V}/V_0$ ) for all five swirlers (from left to right; 810C, 810S, 812C, 816C, 816S, respectively)



**Appendix 2:** Contours of normalized time-averaged x-velocity ( $\bar{U}/V_0$ ) for all five swirlers (from left to right; 810C, 810S, 812C, 816C, 816S, respectively)



**Appendix 3:** Contours of the normalized turbulent kinetic energy ( $TKE/V_0^2$ ) for all five swirlers (from left to right; 810C, 810S, 812C, 816C, 816S, respectively)



**Appendix 4:** Contours of normalized time-averaged y-velocity ( $\bar{V}/V_0$ ) with streamlines for all five swirlers (from left to right; 810C, 810S, 812C, 816C, 816S, respectively)

